

TUHE9582

Rest Frame Valence Quark Model for Deep Inelastic Scattering

J. Franklin and M. Ierano

*Department of Physics, Temple University,
Philadelphia, Pennsylvania 19122, USA*

August 1995

Abstract

A rest frame valence quark model is applied to the deep inelastic scattering of charged leptons by protons. The parameters of the model are determined by a fit to unpolarized electron cross sections. The model then can be used to calculate the asymmetry in polarized deep inelastic scattering. The predicted spin- dependent structure function, g_{1p} , is in good agreement with recent measurements. This indicates that, in the proton rest system, the spin of the proton is carried by the valence quarks.

1. Introduction

The deep inelastic scattering of leptons by protons has been studied since the early 1970's as a tool to investigate the structure of the proton. The near scaling region of about $4 \text{ GeV}^2 < Q^2 < 20 \text{ GeV}^2$ is of interest because this Q^2 is large enough to make the approximation of incoherent scattering by individual quarks reasonable, and most of the accurate unpolarized electron data [1-7] and polarized electron[8, 9] and muon results[10, 11] are for Q^2 in this range.

The standard paradigm for analyzing deep inelastic scattering has been the parton model implemented in the infinite momentum frame. By its nature, the parton model is applicable to the scaling region as $Q^2 \rightarrow \infty$, but is not as effective in the near scaling region where higher twist diagrams are required. The parton model has also led to the strange interpretation of recent polarization experiments that the quark contribution to the spin of the proton is near zero.

An alternative method,[12-17] treating the entire deep inelastic scattering process in the rest frame of the initial proton, was introduced some time ago and shown to be successful in calculating the approach to scaling of the nucleon structure functions as Q^2 increased from 4 GeV 2 up to $q^2 \sim 20$ GeV 2 , where logarithmic QCD corrections become important. The rest frame model also gave an understanding of the behavior of F_{2n}/F_{2p} at large x as arising from SU(6) breaking differences in the u and d quark rest frame wave functions in the proton, and a value for $R=\sigma_L/\sigma_T$ that was consistent with the early experimental estimates [2].

In this paper, we apply the rest frame model to the reanalysis by Whitlow [18] of the early electron data [1-6], which has resulted in more accurate combined cross sections with consistent radiative corrections and a more systematic treatment of the relative normalizations of the different experiments. Fitting the rest frame parameters to these electron cross sections determines the parameters of the model. We then make predictions for the asymmetry observed in polarized lepton-proton deep inelastic scattering, and for the spin dependent structure functions, g_{1p} and g_{2p} , deduced from the polarization asymmetry. We find good agreement with the experimental determinations of g_{1p} , which leads us to conclude that, in the proton rest system, the valence quarks account for the proton spin.

In section 2 of this paper, we describe the rest frame model for unpolarized deep inelastic scattering. Section 3 describes the deep inelastic scattering cross section data, as combined by Whitlow. Our fit to these cross sections is presented in Section 4. In section 5, the rest frame model is extended to the scattering of polarized leptons by polarized protons, and the resulting predictions for the asymmetry and spin dependent structure functions are compared with the polarization data. Section 6 is a general discussion, and our conclusion is presented in Section 7.

2. The rest frame model

2.1. LEPTON-QUARK SCATTERING

The rest frame model treats deep inelastic scattering as the quasi-elastic scattering of the lepton by a point Dirac quark via one-photon exchange. The

initial quark wave function is that of a Dirac particle bound in some potential in the rest frame of the proton. The final state of the struck quark is that of a free quark of mass m . The two spectator quarks will, in general, have some relative momentum distribution characterizing their mutual interaction. In the simple version of the model used here, this momentum distribution is taken to be a delta function so that the spectator quarks appear to be a single diquark of mass M_r . The cross section for deep inelastic scattering of a charged lepton from a proton is then given by the sum of the lepton-quark cross sections, weighted by the quark charges squared. The rest frame model is described in more detail, and contrasted with the usual parton model in I. In the following we present the equations that follow from the model.

Energy conservation in the proton rest system is given by

$$1 + \nu = E' + E_r, \quad (1)$$

with

$$E' = [(\vec{p} + \vec{q})^2 + m^2]^{1/2}, \quad (2)$$

$$E_r = (\vec{p}^2 + M_r^2)^{1/2}, \quad (3)$$

where $q^\mu = (\nu, \vec{q})$ is the lepton four-momentum loss (or the virtual photon four-momentum) and \vec{p} is the Fourier transform variable for the initial quark wave function. (This can be thought of as the initial quark momentum.) We use units in which the proton mass $M_p=1$. The recoil energy, E_r of the two spectator quarks introduces the effective recoil mass M_r as a parameter of the model. The photon laboratory energy ν can be put into Lorentz invariant form as $\nu = P \cdot q$, where P^μ is the initial proton four-momentum, given in the laboratory by $(1, \vec{0})$.

The lepton scattering calculation is straightforward (see the appendix of I). The laboratory cross section for the scattering of a charged lepton of four momentum $k^\mu = (\omega, \vec{k})$ into $k'^\mu = (\omega', \vec{k}')$ by a bound quark of unit charge is given by

$$\frac{d^2\sigma}{d\Omega d\omega'} = \left(\frac{\omega'}{\omega}\right) \frac{1}{2\pi^2} \int \frac{d^3p |\phi(p)|^2 |\mathcal{M}|^2}{E_+ E'} \delta(E' + E_r - 1 - \nu), \quad (4)$$

where $\phi(p)$ and E_+ are defined in terms of the initial quark Dirac momentum wave function

$$\Phi(\vec{p}) = \begin{pmatrix} \chi \\ \frac{\sigma \cdot \vec{p}}{E_+} \chi \end{pmatrix} \phi(p), \quad (5)$$

where χ is a constant Pauli spinor. In I the denominator of the small components of the bound Dirac wave function, E_+ , was approximated as a constant parameter of the calculation. In the present application of the rest frame model, we use a more realistic bound state wave function for which E_+ is the appropriate function of the momentum p . The Dirac momentum wave function is normalized so that

$$\int d^3p \Phi^\dagger \Phi = 1, \quad (6)$$

which is different than in I where the scalar wave function ϕ was normalized to 1. For this reason, Eq.(4) is slightly different than Eq. (4) of I. With the present normalization, the sum over spins of the initial bound quark results in the positive energy projection operator

$$\Lambda = \frac{\bar{p} + \bar{m}}{E_+}, \quad (7)$$

which accounts for the $1/E_+$ in Eq. (4). The matrix element squared is given by

$$|\mathcal{M}|^2 = [(4\pi\alpha)^2/2Q^4][(p' \cdot k')(\bar{p} \cdot k) + (p' \cdot k)(\bar{p} \cdot k') - m\bar{m}(k \cdot k')], \quad (8)$$

where

$$\vec{p}' = \vec{p} + \vec{q}, \quad p'^0 = E', \quad \bar{p}' = \vec{p}, \quad \bar{p}^0 = \bar{E}, \quad (9)$$

$\alpha=1/137$, and $Q^2 = -q^2$. We neglect the lepton mass throughout.

A departure from the free particle matrix element is the appearance of the quantities \bar{E} and \bar{m} in Eqs. (7-9). \bar{E} is the energy component of the four-vector p^μ and, for a free quark, would be the quark energy. However for a bound quark, \bar{E} is not the energy, but direct calculation with the Dirac equation shows that \bar{E} can be written as

$$\bar{E} = (E_+^2 + \vec{p}^2)/2E_+. \quad (10)$$

\bar{m} behaves like an effective mass of the bound quark in the initial state and is given by

$$\bar{m} = (E_+^2 - \vec{p}^2)/2E_+. \quad (11)$$

The angular integration in Eq. (4) can be performed by using the energy delta function to fix $\cos\theta_{pq}$ with the result

$$\frac{d^2\sigma}{d\Omega d\omega'} = \frac{\omega'}{\pi\omega|\vec{q}|} \int_{p_m}^{p_M} \frac{pd\vec{p}}{E_+} |\phi|^2 \overline{|\mathcal{M}|^2}, \quad (12)$$

where $\overline{|\mathcal{M}|^2}$ is averaged over φ_{pq} . The limits on the integral, p_m and p_M , are the minimum and maximum momenta, respectively, for which the δ function argument can vanish. The minimum momentum p_m is given by the solution to the quadratic equation that arises when the energy conservation equation (1) is solved for \vec{p} with \vec{p} and \vec{q} antiparallel. In most cases, the maximum momentum p_M is the solution for \vec{p} and \vec{q} parallel, but there are cases for which $\cos\theta_{pq}$ never reaches 1 and then p_m and p_M are two separate solutions of Eq. (1) with $\cos\theta_{pq} = -1$. The maximum momentum is always greater than ν and can usually be approximated as infinite.

Equation (12) gives the cross section for the scattering of a charged lepton by a bound Dirac quark of unit charge. If we assume that the proton is made up of three Dirac quarks with charges q_i such that $\sum_i q_i^2 = 1$, that scatter incoherently, then Eq. (12) can be considered the cross section for inelastic lepton-proton scattering. This assumes identical wave functions for the quarks. In Ref. [12] we emphasized that the u and d quarks should have quite different wave functions in the proton, corresponding to a diquark-like clustering [19-21]. However, since the two u quarks contribute $\frac{8}{9}$ of the cross section and the d quark only $\frac{1}{9}$, it turns out to be a good approximation, for the proton, to take all quark wave functions the same. In lepton-deuteron scattering, where the neutron is included, there is a large dependence on the d quark wave function and different d and u quark wave functions are required to fit scattering by deuterons [12,16].

The assumption of incoherent scattering is not an essential one, and interference effects could be calculated if we used a three body wave function instead of the effective one body wave function approach described here. This would permit comparison with lower Q^2 data, but would be a much more complicated calculation. The importance of coherence effects depends on the ratio $|\vec{p}|/|\vec{q}|$ and this is always very small for the range $Q^2 > 4 \text{ GeV}^2$ considered in this paper.

2.2 THE PROTON STRUCTURE FUNCTIONS F_1 AND F_2

In this paper we fit the lepton-proton inelastic cross section of Eq. (12) directly to experimental cross sections, but it is still of interest to identify the proton structure functions $F_1(x, Q^2)$ and $F_2(x, Q^2)$, where x is the usual Bjorken scaling variable

$$x = Q^2/2\nu. \quad (13)$$

These can be identified by writing the cross section as

$$\frac{d^2\sigma}{d\Omega d\omega'} = \frac{\omega'\alpha^2}{Q^4\omega\nu} [4\omega\omega'F_2 + Q^2(2\nu F_1 - F_2)]. \quad (14)$$

In the Bjorken scaling limit, $\nu \rightarrow \infty$, $Q^2 \rightarrow \infty$, with x fixed, F_1 and F_2 become functions of x alone given by

$$F_1(x) = 2\pi \int_{p_m(x)}^{\infty} (p/E_+) dp |\phi(p)|^2 (\bar{E} + E_r - 1 + x) \quad (15)$$

$$F_2(x) = 2xF_1(x), \quad (16)$$

with the minimum momentum depending only on x through

$$p_m(x) = \frac{1}{2} |1 - x - M_r^2/(1 - x)|. \quad (17)$$

Thus the rest frame model leads to the same scaling limit as the usual parton model. There is no $\log(Q^2)$ scale breaking in the present model because the final state quark is taken to be free. Introducing a QCD final state interaction between quarks would lead to such $\log(Q^2)$ scale breaking that would be important at high Q^2 . However, for Q^2 less than 20 GeV 2 , any $\log(Q^2)$ effect would be masked by the larger Q^2 dependence in Eqs. (19) and (20) below.

It can be seen from Eq. (15) that quark binding has a large effect on the structure functions, even in the scaling limit. Without binding, E_+ would be a constant (2m), and energy conservation would give $\bar{E} + E_r = 1$. Then F_1 and F_2 would be simply related to the quark wave function and sum rules could be derived, similar to those that follow in the parton model. However, with binding, these sum rules cannot be derived in the rest frame model.

For finite ν and Q^2 , the approach to scaling is given to all orders in $1/\nu$ by

$$F_i(x, Q^2) = 2\pi(1 + 2x/\nu)^{-\frac{1}{2}} \int_{p_m(x,\nu)}^{p_M(x,\nu)} (p/E_+) dp |\phi(p)|^2 f_i(x, \nu, p). \quad (18)$$

The integrand functions f_i are given by

$$f_1 = \bar{E}(1 - m/\nu) + \tilde{p}_L[1 + (2x - 1 + E_r - \bar{E})/\nu] - (\tilde{p}_L^2/\nu)(2 + x/\nu) + (p^2/E_+)(m/\nu) - p^2x/(\nu^2 + 2x\nu) + f_2/2\nu, \quad (19)$$

$$f_2 = 2[\bar{E}(1 - E_r) - \tilde{p}_L(E_r - \bar{E} - 1) + \tilde{p}_L^2(1 - x/\nu) + p^2x/(\nu + 2x)] \quad (20)$$

where $\tilde{p}_L = p_L/\sqrt{1 + 2x/\nu}$, and p_L is the quark longitudinal momentum given by

$$p_L = -pcos\theta_{pq} = [x - 1 + E_r(1 + 1/\nu) - (1 + M_r^2 - m^2)/2\nu]/\sqrt{1 + 2x/\nu}. \quad (21)$$

The minimum and maximum momenta for the integral are now non-scaled functions of x and ν . We use the non-scaled structure functions of Eq. (18) in Eq. (14) to fit the experimental cross sections.

2.3 QUARK WAVE FUNCTION

Because the integrals in Eq. (18) are over a large range of momentum, the structure functions do not depend sensitively on the quark wave function. It turns out that any relativistic wave function that falls off in momentum with a power of about p^5 can fit the deep inelastic data, and in I a simple power law momentum wave function with a constant denominator for the small components gave a reasonable fit to the SLAC data. In order to get a more consistent relativistic relation between the large and small components, and to more accurately reflect the dominance of the one gluon exchange potential in the momentum range of our integrals, we use a Dirac wave function for a Coulomb potential. While the actual one gluon potential of a single quark in the three quark system is more like a screened Coulomb, we feel that the use of a Coulomb potential to connect large and small components is sufficient in this case. This is especially true since we do observe that the structure functions are not sensitive to the exact details of the wave function. We find that using bag model wave functions or relativistic Gaussian wave functions in the integrals turns out to give a poor fit to the deep inelastic cross sections.

The Dirac-Coulomb wave function in momentum space is given by Eq. (5), with the scalar part given by

$$\phi^2(p) = \frac{b(b+1)(2a)^{2b+1}\Gamma^2(b)\sin^2[(b+1)\tan^{-1}(p/a)]}{8\pi^2\Gamma(2b)p^2(p^2+a^2)^{b+1}}. \quad (22)$$

$\phi(p)$ is the Fourier transform of the scalar spatial wave function

$$\psi(r) = Nr^{b-1}e^{-ar}. \quad (23)$$

The wave function depends on two parameters: a , the size parameter, and b which determines the singularity at the origin of the Dirac wave function. In momentum space, a gives the width of the momentum distribution, and b determines the power of the asymptotic p behavior. The denominator of the small components in the momentum wave function is given by

$$E_+ = \frac{p^2b[(1+b)/(1-b)]^{\frac{1}{2}}}{a - (1+b)pcot[(1+b)\tan^{-1}(p/a)]}. \quad (24)$$

In I it was shown that, if $\phi^2 \sim p^{-5}$ at large p , then F_2 would behave like $(1-x)^3$ as $x \rightarrow 1$, as has been suggested by perturbative QCD and also noted experimentally. This corresponds to $b=\frac{1}{2}$, for which the momentum wave function could be written in the simpler form

$$\phi^2 = \frac{3a^2[2a + \sqrt{p^2 + a^2}]^2}{16\pi(p^2 + a^2)^3[a + \sqrt{p^2 + a^2}]} \quad (25)$$

and

$$E_+ = \sqrt{3}a + \frac{\sqrt{3}(p^2 + a^2)}{2a + 3\sqrt{p^2 + a^2}}. \quad (26)$$

The rest frame model thus depends on two wave function parameters, a and b , and two masses, the final state quark mass m and the final state effective recoil mass M_r . The mass of the struck quark in the initial state is masked by the function \bar{m} which acts as an effective mass in the scattering matrix element.

3. The deep inelastic scattering cross sections

Most of the accurate data for unpolarized electron-proton deep inelastic scattering was taken some time ago at SLAC by several different groups using different experimental techniques and beams [1-7]. Different methods were also used for radiative corrections. The differences in radiative corrections and the lack of good relative normalizations between different experiments led to large uncertainties in the separation of the two proton structure functions and the determination of the ratio $R = \sigma_L/\sigma_T$. Recently, these experiments have been reanalyzed by Whitlow [18] using the same radiative correction technique for each experiment. A careful evaluation was also made of the relative normalizations of the various experiments. The Whitlow analysis has resulted in a consistent set of combined experimental cross sections measured in six different experiments [1-6] over a relatively wide range of kinematical variables.

Until now, the meeting ground of theory and experiment for deep inelastic scattering has been at the level of the structure functions. That is, the experimentalists used *ad hoc* parameterizations of the data to produce “experimental” structure functions which were then used to test theoretical predictions. But these structure functions are not truly experimental quantities. They include arbitrary theoretical constructs in their determination. This situation has been much improved with the Whitlow analysis, but the resulting structure functions still are not direct experimental quantities.

For this reason, we fit our rest frame model directly to the Whitlow cross sections so that the theory is tested directly at the experimental level. The fit to the experimental cross sections determines the parameters of the rest frame model, which can then be used to determine the separated structure functions F_1 and F_2 , the ratio R , and details of the approach to scaling for Q^2 in the range 4-20 GeV 2 . We can also use the model, with its parameters fixed by the unpolarized fit, to predict the asymmetry in polarized lepton-proton deep inelastic scattering and the spin dependent structure functions g_1 and g_2 to compare with recent experiments[9,11].

As mentioned earlier, the relative normalization of the different experiments is of great importance in separating the two structure functions. For the small angle experiments [1-4,6] at 6-34° there is enough overlapping deep inelastic data so that Whitlow could find unambiguous relative normaliza-

tions. However the wide angle experiment [5] at 50° and 60° had no deep inelastic points near the smaller angle experiments. At the same time, the wide angle data, precisely because it was in such a different kinematical region, is the most sensitive for separating F_1 and F_2 . In an attempt to arrive at some reasonable estimate of the wide angle normalization relative to the lower angle experiments, Whitlow used available elastic scattering comparisons. But this involved assuming a scaling hypothesis for the elastic form factors G_E and G_M that has not been tested in this region, so that this relative normalization was more uncertain than the others.

Our procedure in fitting the rest frame model to experiment has been to treat all normalizations as experimental quantities to be fit, as well as fitting each experimental point. That is, we fit to the combined Whitlow data by minimizing the following χ^2 function

$$\chi^2 = \sum_i^{119} \left(\frac{\sigma_i - \sigma_i^W}{\Delta_i} \right)^2 + \sum_{j \neq 2}^6 \left(\frac{N_{j2} - N_{j2}^W}{\Delta N_{j2}} \right)^2 + \left(\frac{N_2 - N_2^W}{\Delta N_2} \right)^2. \quad (27)$$

The superscript W refers to Whitlow, but the cross sections σ_i^W in Eq. (27) use our normalization N_j instead of Whitlow's N_j^W . (The subscript j refers to Refs. 1-6 and i refers to each experimental point.) The experimental error Δ_i is that in Whitlow file E.2 with his normalization error taken out, while ΔN_{j2} and ΔN_2 are the errors given in Whitlow table (5.2) as the experimental errors on the normalization determinations, N_{j2}^W and N_2^W , given in that table. Only N_2 , the normalization for Ref. 2 is an absolute normalization. Following Whitlow, the other normalizations are relative normalizations N_{j2} . We vary N_2 and the N_{j2} separately. It is an important feature of our fit to treat the normalization errors as normalization errors in this way, and not to include them in the point to point errors.

4. Results for unpolarized scattering

4.1 CROSS SECTION FIT

The rest frame model described in section 2 depends on four parameters: a, the size parameter for the quark wave function; b, which determines the exponent of the asymptotic momentum dependence of the wave function;

M_r , the effective recoil mass of the spectator quark system; and m , the final quark mass. We have fit this model to the Whitlow combined cross sections by minimizing the χ^2 function in Eq. (27) with respect to the four model parameters a , b , M_r , m , and five normalizations. There is one absolute normalization and four relative normalizations. (None of the data points from Ref. 3 survived the cuts described below.) In making this fit, we have made cuts on the range of kinematical variables for which we believe the rest frame model should apply. Specifically, we fit only to data in the ranges

$$Q^2 > 4\text{GeV}^2 \quad (28)$$

$$W > 3.1\text{GeV} \quad (29)$$

$$x > 0.3. \quad (30)$$

W is the total invariant mass of the final hadronic state given by

$$W^2 = 1 + [(1 - x)/x]Q^2. \quad (31)$$

We have determined these ranges by the values of the respective parameters below which $\Delta\chi^2/\Delta$ DF shows a rapid rise. The values at which this happens are reasonable, considering the expected range of validity of the rest frame model. The Q^2 cut is required so that the incoherence assumption will be satisfied. The W cut is required to leave out direct resonance production (quasi-elastic) which is not included in the model. The W cut is not as necessary for Q^2 above about 10 GeV^2 , where the quasi-elastic form factor effectively eliminates this background. The x cut is required because other modes of deep inelastic scattering in addition to the electron-quark direct scattering mechanism seem to become effective at small x . In I we attributed this mainly to quark pair production, which is the rest frame equivalent of the sea in the parton model.

With these cuts, we fit 119 of the points in the combined Whitlow set, and obtain a χ^2 of 198 for 110 degrees of freedom (DF). Our best fit values are

$$a = 393\text{MeV} \quad (32)$$

$$b = 0.515 \quad (33)$$

$$M_r = 0.968M_p, \quad (34)$$

$$(35)$$

with the best quark mass being zero. The value of χ^2 increases slowly with increasing quark mass, reaching 217 at $m=300$ MeV (with little change in the other parameters), which still represents a reasonable fit.

The χ^2 for the best fit is larger than the degrees of freedom. This is due to the considerable reduction in the error bars achieved in the Whitlow combined fit compared to that of the original experiments. Earlier fits of the model to the original data gave a χ^2 that was less than the degrees of freedom. With the smaller errors, our simple model cannot fit every nuance of the data, but the overall fit is quite good. This is illustrated by two sample cross section comparisons in Fig. 1. (There are 34 such plots that make our cuts, but some have only one or two points within the cut.) Figures 1a and 1b show reasonable agreement, but have relatively high χ^2 . The χ^2/DF , calculated only for the points within our cuts (square data points), for Fig. 1a is 12/6, and it is 10/7 for Fig. 1b. Figure 1a represents the typical way in which the rest frame model deviates from experiment beyond our cuts (circled data points, which were not included in the fit). The model is usually below experiment for $x < 0.3$, suggesting that other production modes are effective. The model is also below the data for $W < 3.1$ GeV where resonance production, which is not included in the model, is taking place. In some cases, this disagreement with experiment for $W < 3.1$ GeV (at large x) is not evident in the plot, but, because of the small error bars, would lead to a large increase in χ^2 .

There are five independent normalizations in the Whitlow combined fit. These are the absolute normalization, N_2 , of experiment 2, and four relative normalizations N_{j2} . Our fit to the relative normalizations, N_{j2} , $j \neq 5$, which Whitlow could base on overlapping inelastic data, all agree with his normalizations. But our fit to the wide angle relative normalization, N_{52} , is somewhat different than Whitlow's, which was based on elastic scattering comparisons and involved some theoretical assumptions. Our best fit normalization is $N_{52}=1.064$, whereas Whitlow had $N_{52}^W = 1.008 \pm .028$. This difference contributes 4 to our overall χ^2 in Eq. (27). Whitlow's absolute normalization for experiment 2 also could not be based on overlapping data. Our fit to that normalization is $N_2=0.919$, compared to $N_2^W = 0.981 \pm .021$, and contributes 9 to our overall χ^2 .

It is important that the wave function fall off asymptotically like a power of p close to $\frac{5}{2}$, which leads to $F_2(x) \sim (1-x)^3$ as $x \rightarrow 1$. Gaussian and bag model wave functions do not give reasonable fits to the deep inelastic

cross sections, especially at large x , because they do not have this power law momentum dependence. For our wave function, the large x behavior is given by $F_2(x) \sim (1 - x)^{2(b+1)}$. The value $b=\frac{1}{2}$ would correspond in the Dirac-Coulomb wave function to a coupling strength $\lambda=\sqrt{3}/2$. If the two spectator quarks were represented by a point diquark, this would correspond to a strong coupling constant $\alpha_S=\frac{3}{4}\lambda=0.66$. This is a bit below an estimate from baryon mass splittings of $\alpha_S=0.96$ [22]. The smaller α_S found here is a reasonable result of the spectator quarks being more spread out than a point diquark.

The quark wave function is also related to the initial mass, m_i , of the struck quark. Our value of $a=393$ MeV corresponds to $m_i+S=2a/\sqrt{3}=450$ MeV, where S is the average value of a confining potential, represented in our model wave function as a constant Lorentz scalar potential. This permits a reasonable range of quark masses and confining potentials.

More complicated wave functions could be used with more realistic spectator quark distributions and a linear confining potential. We do not feel that this would appreciably improve the fit, although it could modify the quark model size and mass parameters.

4.2 STRUCTURE FUNCTIONS

Once the parameters of the model have been set by fitting to the experimental cross-sections, we can calculate the structure functions F_1 and F_2 as functions of the invariants. Figure 2 shows F_2 as a function of Q^2 for several values of x , along with the Whitlow determinations (data points) of F_2 . We emphasize that this is not a comparison of theory with experiment, but a comparison of two different methods of extracting the structure functions from the same experimental cross sections. The points plotted exclude the region with W less than 3.1 GeV for which there would be quasi-elastic resonance production, which is not included in our model. The agreement in x and Q^2 is reasonable, except for the wiggle in the Whitlow extraction at $x=0.35$, which would be hard to reproduce in any simple model.

Another quantity of interest is the ratio $R=\sigma_L/\sigma_T$, which is related to F_1 and F_2 by

$$R = (1 + 2x/\nu)F_2/2xF_1 - 1. \quad (36)$$

R should approach zero in the scaling limit. The early experimental determinations [2,4,6] had large errors because the experiments covered a small

range (6-30°) of angles and the different experiments had uncertain relative normalizations. The Whitlow analysis of the early experiments readjusted the relative normalizations to make them compatible where they overlap, and have added experimental cross sections [5] at 50° and 60°, but with a more uncertain relative normalization.

We compare our determination of R with that of Whitlow (data points) in Fig. 3. These, also, represent two different extractions of R from the same cross sections. There is reasonable agreement, although there is considerable scatter in the Whitlow R extraction. The agreement continues even into the low W region.

5. Polarized deep inelastic muon scattering

5.1 POLARIZATION EXPERIMENTS

The polarized deep inelastic scattering experiments [8-11] have generally measured the asymmetry in the scattering of charged longitudinally polarized leptons by longitudinally polarized protons. (Ref.[9] also measured transverse asymmetry.) Specifically, they have measured the quantity

$$A = \frac{\frac{d^2\sigma^{\uparrow\downarrow}}{d\Omega d\omega'} - \frac{d^2\sigma^{\uparrow\uparrow}}{d\Omega d\omega'}}{\frac{d^2\sigma^{\uparrow\downarrow}}{d\Omega d\omega'} + \frac{d^2\sigma^{\uparrow\uparrow}}{d\Omega d\omega'}} \quad (37)$$

where the arrows refer to the initial lepton and proton spin projections along the incident lepton direction in the laboratory. The denominator of Eq. (37) is just twice the unpolarized cross section given by Eq. (12).

Dimensionless spin dependent structure functions g_1 and g_2 can be defined in terms of the numerator of Eq. (37) by

$$\begin{aligned} \mathcal{N} &= \frac{d^2\sigma^{\uparrow\downarrow}}{d\Omega d\omega'} - \frac{d^2\sigma^{\uparrow\uparrow}}{d\Omega d\omega'} \\ &= \frac{4\alpha^2\omega'}{Q^2\nu} \left(\left[2 - \frac{\nu x}{\omega^2} \right] g_1(x, Q^2) - \frac{\nu}{\omega} [g_1(x, Q^2) + \frac{2x}{\nu} g_2(x, Q^2)] \right). \end{aligned} \quad (38)$$

The measured asymmetries can be given in terms of the virtual photon

asymmetry

$$A_1 = \frac{\sigma_{\frac{1}{2}} - \sigma_{\frac{3}{2}}}{\sigma_{\frac{1}{2}} + \sigma_{\frac{3}{2}}}, \quad (39)$$

where σ_J is the virtual photon-proton absorption cross section with total spin projection J along the photon momentum. A_1 is related to the structure functions by

$$A_1 = (g_1 - 2xg_2/\nu)/F_1. \quad (40)$$

5.2 REST FRAME MODEL FOR POLARIZED SCATTERING

The rest frame model treats lepton-quark scattering which gives \mathcal{N}_{quark} , and this must be related to \mathcal{N}_{proton} . There is a depolarization of the quarks with respect to the proton polarization. This depolarization follows from the proton spin wave function

$$P \uparrow> = \frac{1}{\sqrt{6}}(2 \uparrow\uparrow\downarrow - \uparrow\downarrow\uparrow - \downarrow\uparrow\uparrow), \quad (41)$$

where the order (uud) is understood for the valence quarks constituting the proton. The polarized lepton- proton cross sections are the sum of the lepton-quark cross sections, weighted by the squares of the quark charges. This leads to

$$\sigma_{proton}^{\uparrow\uparrow} = \frac{1}{9}(7\sigma^{\uparrow\uparrow} + 2\sigma^{\uparrow\downarrow})_{quark} \quad (42)$$

$$\sigma_{proton}^{\uparrow\downarrow} = \frac{1}{9}(2\sigma^{\uparrow\uparrow} + 7\sigma^{\uparrow\downarrow})_{quark}, \quad (43)$$

and, from Eq. (37)

$$A_{proton} = \frac{5}{9}A_{quark}. \quad (44)$$

As in the unpolarized case, we have assumed the same momentum wave function for the u and d quarks.

The polarized lepton-quark cross section calculation proceeds like the unpolarized calculation, but with spin projection operators inserted into the

initial lepton and quark matrix elements. The spin projection operators are given by

$$\Lambda_\uparrow = \frac{1}{2}(1 + \gamma^5 \gamma_\mu W^\mu), \quad (45)$$

where W^μ is the covariant spin vector for polarization in the \hat{k} direction, given by

$$\overline{m}W_p^\mu = [\vec{p} \cdot \hat{k}, (\vec{p} \cdot \hat{k})(\vec{p}/E_+) + \overline{m}\hat{k}] \quad (46)$$

for the initial struck quark, and

$$m_L W_L^\mu = (\omega, \vec{k}) \quad (47)$$

for the lepton. The lepton mass m_L has been neglected on the right hand side of Eq. (47).

The resulting matrix element squared for polarized lepton-quark scattering is

$$\begin{aligned} |\mathcal{M}^{\uparrow\uparrow}|^2 = & [(4\pi\alpha)^2/2Q^4] \{ [(k' \cdot p')(k \cdot \bar{p}) + (k' \cdot \bar{p})(k \cdot p') - m\overline{m}(k \cdot k')] \\ & + m_L \overline{m} [(W_L \cdot W_p)(-q \cdot p') + (W_L \cdot p')(W_p \cdot q)] \\ & + m_L m [(W_L \cdot W_p)(-q \cdot \bar{p}) + (W_L \cdot \bar{p})(W_p \cdot q)] \}. \end{aligned} \quad (48)$$

$|\mathcal{M}^{\uparrow\downarrow}|^2$ is given by Eq. (48) with W_p replaced by $-W_p$. Then, repeating the steps of the unpolarized calculation leads to polarized cross sections from which g_1 and g_2 can be identified using Eq. (38).

$$g_i(x, Q^2) = \left(\frac{5}{9}\right) 2\pi (1 + 2x/\nu)^{-\frac{1}{2}} \int_{p_m}^{p_M} (p/E_+) dp \phi^2 h_i, \quad (49)$$

with the factor $\frac{5}{9}$ coming from the depolarization in Eq. (44). The integrand functions are given by

$$\begin{aligned} h_1 = & \overline{m} + \tilde{p}_L (1 - \overline{m}/\nu) + (\tilde{p}_L^2/E_+) [1 - (E_r + E_+ - 1)/\nu] \\ & + (\tilde{p}_T^2/2E_+) [1 + (E_+ + E_r - 1 + 2x)/\nu] \\ & + (m/\nu) (\tilde{p}_L + \tilde{p}_L^2/E_+ - \tilde{p}_T^2/2E_+) \end{aligned} \quad (50)$$

$$\begin{aligned} h_2 = & \frac{1}{2x} [\overline{m}(E_r - 1 + 2x) + \overline{m}\tilde{p}_L (1 + 2x/\nu)] \\ & + (p_T^2/2E_+) (E_+ + E_r - 1 + 2x) \\ & - \frac{m}{2x} [\overline{E} + \tilde{p}_L (1 + 2x/\nu) - p_T^2/2E_+] - h_1. \end{aligned} \quad (51)$$

The parameters of the model have been set by the fit to the unpolarized cross sections, so that the polarization predictions have no adjustable parameters. It can be seen again, from Eqs. (50) and (51), that, due to binding effects, the connection of g_{1p} to the quark wave function is not simple enough to derive parton model type sum rules for the integral of g_{1p} , even in the scaling limit.

5.3 POLARIZATION RESULTS

The virtual photon asymmetry A_1 is plotted in Fig. (4). The experimental points are from the SMC muon experiment[11] (solid points) and the SLAC E143 electron experiment[9] (open points). The square points in each case are within the $x > 0.3$, $W > 3.1$ GeV, $Q^2 > 4$ GeV 2 range of the rest frame model. The SMC data was taken at much higher Q^2 than the E143 data. The curve is the rest frame prediction for A_1 , calculated at each E143 point for the actual Q^2 at that point. The rest frame model is in reasonable agreement (We discuss the jump in the E143 asymmetry around $x=0.4$ later.) with these experiments in the range $x > 0.3$, but, for $x < 0.3$ the predicted asymmetry is much above that of both experiments. This is because the calculated unpolarized cross section in the denominator of the asymmetry definition Eq. (37) is too small in the rest frame model for $x < 0.3$.

In Fig. 5a our predictions for g_{1p} , which is related only to the difference of cross sections, is shown along with the SMC experimental values. Our calculations for g_{1p} are made at the experimental value of Q^2 for each data point. The solid triangle on the x axis shows the x value below which Q^2 is less than 4 GeV 2 .

The rest frame prediction of this paper (dashed curve), gives a χ^2 of 24 for the 12 SMC data points, including all the points on the curve. In Ref. [16], it was shown that different d and u quark wave functions are required to simultaneously fit unpolarized deuteron and proton cross sections. Using those different d and u wave functions has little effect on the unpolarized proton cross section, but decreases the proton g_1 at small x (solid curve), improving χ^2 to 14 for the 12 data points in Fig. 5a. We interpret this good agreement, even below $x=0.3$, to mean that the higher diagrams left out of our calculation do not contribute much to the polarization and their effect cancels out of the difference between polarized cross sections. The

improvement of the prediction for different u and d quark distributions shows that the polarized scattering is a more sensitive test of SU(6) breaking in the proton than is the unpolarized scattering.

Figure 5b shows the SLAC E143 measurement of g_{1p} , along with the rest frame predictions for the same (dashed curve), and different (smooth curve) u and d quark distributions. The E143 g_{1p} was evaluated at a constant $Q^2=3.0$ GeV 2 for each x, and we use that Q^2 in our calculation for this figure. Again, different u and d distributions give a better prediction for g_{1p} .

In Fig. 5b, the solid triangle on the x axis indicates the point below which $Q^2 < 4$ GeV 2 , and the open triangle the point above which $W > 3.1$ GeV 2 . We attribute the jump in the E143 g_{1p} around $x=0.4$ to quasi-elastic production of resonances at these lower values of W. The lowest x point in the jump at $x=0.416$ has $W=3.3$, just above our chosen cutoff of $W=3.1$ GeV. The five higher x points all have $W < 3.1$ GeV. In fitting the unpolarized cross sections, the W cutoff was chosen somewhat arbitrarily, since resonance production does not set in at one particular energy. There is only one SMC point in this x range. We show that by the open circle at $x=0.48$. This SMC point has $W=8$ GeV and $Q^2=58$ GeV 2 . By contrast, the E143 point at $x=0.47$ has $W=3.04$ GeV and $Q^2=7.4$ GeV 2 . It will be interesting to see if future data in this x region comes down to the SMC level as W and Q^2 are increased.

Figure 6 shows the rest frame prediction for g_{2p} . It is seen to be very small until x gets below about 0.01. Even though g_2 gets quite large at small x, it is multiplied by x/ν in Eq. (38) for \mathcal{N} , and does not affect the extraction of g_1 from longitudinal asymmetries.

6. Discussion

The version of the rest frame model presented here is quite simple in that we have used a simple two parameter wave function, and a delta function approximation of the spectator quark relative momentum distribution. We have also calculated only the lowest order diagram, which restricts our model to the range of $x > 0.3$. In that range, the cross section fit looks quite good, as indicated by Fig. 1.

The model could be extended in a number of ways:

1. A more sophisticated wave function could be used. The fit is already good enough that we do not feel that this is warranted, and a better wave function would probably not extend the range of validity, although it could affect the best fit quark model parameters.
2. The additional process of quark pair production by the virtual photon, followed by quark (or anti-quark) scattering via QCD could be included. This could extend the validity of the model below $x=0.3$. The quark pair diagram in the rest frame corresponds to the quark-antiquark sea in the infinite momentum frame. That is, the rest frame model does not have a $q - \bar{q}$ sea, but the pair production diagram would contribute. While at infinite momentum, the quark pair diagram (a so called z-graph) does not contribute, but a $q - \bar{q}$ sea is generally introduced at low x . In each case, the simple valence quark model does not contribute enough at low x .
3. Gluon bremsstrahlung and final state interaction between the quarks via one gluon exchange could be included. This would lead to the logarithmic Q^2 dependence, characteristic of QCD. Without this final state interaction, the simple model used here has pure scaling in x as Q^2 becomes large.
4. Different u and d quark wave functions should be used. This is not too important for the proton where the d quarks contribute only $\frac{1}{9}$ to the cross section, but is needed to describe the deuteron and the x dependence of the ratio F_{2n}/F_{2p} [12,16]. We have also shown in Fig. 5 that different u and d quark distributions improve the prediction for g_{1p} .

The rest frame model used here is very much like the parton model in its application to experiment. Our structure functions have the same experimental application as those of the parton model. However, the proton looks quite different in the two models. In the rest frame model, the proton wave function is simple, with only the three valence quarks. In the parton model, implemented in the infinite momentum frame (or on the light cone), the dynamics is simpler, but the wave function more complicated in having an explicit gluon component and a $q - \bar{q}$ sea. Since the results of each model can

be presented in terms of Lorentz invariants, they must be equivalent in some sense. We believe that their equivalence lies in the quark pair diagrams in the rest frame model corresponding to the sea at infinite momentum, and the gluons at infinite momentum corresponding to the Lorentz transformation of the internal energy of the rest frame quarks.

In its polarization predictions, the rest frame model seems particularly clearer. Our success in predicting the measured g_{1p} , even at low x , indicates that the complicating diagrams in the rest frame do not contribute to the polarization, which is accounted for completely by the valence quarks. While in the parton model, the sea and the gluon component both seem to be highly polarized so that there is no simple understanding of the origin of the proton spin. One could say that the rest frame model is lucky in that the mechanisms left out of the model (at this stage) do not seem to contribute to the polarization, while the parton model is unlucky in this respect.

6. Conclusion

The simple version of the rest frame model presented here has given a reasonable fit to the unpolarized deep inelastic cross sections. With the model based on this unpolarized fit, we find good agreement with polarization measurements of the spin dependent structure function g_{1p} of the proton. We conclude from this that deep inelastic scattering can be understood by looking at the proton, in its rest system, as composed of three relativistically bound valence quarks, with the spin of the proton carried completely by the valence quarks.

One of us (JF) would like to thank Temple University for a Research Leave and the Lady Davis Fellowship Trust for a Lady Davis Fellowship at the Technion where part of this work was performed.

References

- [1] J. S. Poucher, *et al.*, Phys. Rev. Lett. **32** (1974) 118

- [2] E. M. Rordan, PhD thesis, MIT-LNS RX-648, unpublished (1973); SLAC-PUB-1643, unpublished (1975).
- [3] S. Stein, *et al.*, Phys. Rev. **D12** (1975) 1884
- [4] A. Bodek *et al.*, Phys. Rev. **D20** (1979) 1471
- [5] W. B. Atwood *et al.*, Phys. Lett. **64B** (1976) 479
- [6] M. D. Mestayer *et al.*, Phys. Rev. **D27** (1983) 285
- [7] G. Miller *et al.*, Phys. Rev. **D5** (1972) 528
- [8] G. Baum *et al.*, Phys. Rev. Lett. **51** (1983) 1135
- [9] K. Abe *et al.*, Phys. Rev. Lett. **74** (1995) 346.
- [10] J. Ashman *et al.*, Phys. Lett. **B206** (1989) 1135; Nucl. Phys. **B328** (1989) 1.
- [11] B. Adeva *et al.*, Phys. Lett. **B302** (1993) 533.
- [12] J. Franklin, Phys. Rev. **D16** (1977) 21
- [13] J. Franklin, Nucl. Phys. **B138** (1978) 122. We refer to this paper as I.
- [14] L. Conci and M. Traini, Few Body Systems **8** (1990) 123
- [15] M. Traini, L. Conci, and Moschella, Nucl. Phys. **A544** (1992) 731
- [16] M. Ierano and J. Franklin Bull. Am. Phys. Soc. **36** (1991) 1246; M. Ierano, Temple University Ph.D. thesis, unpublished (1991).
- [17] J. Franklin and M. Ierano, in *Weak and Electromagnetic Interactions in Nuclei* (WEIN-92) (World Scientific, Singapore, 1992), Ed. Ts. D. Vylov, pp. 515-520.
- [18] L. W. Whitlow, Stanford Ph.D. thesis (1990); SLAC-Report-357, unpublished (1990).
- [19] D. B. Lichtenberg and L. J. Tassie, Phys. Rev. **155** (1967) 1601.
- [20] J. Franklin, Phys. Rev. **D21** (1980) 241.

[21] I. M. Narodetski, Yu. A. Simonov, V. P. Yurov, ITEP (Moscow) preprint ITEP-92-39, (1992).

[22] J. Giammarco and J. Franklin, Nucl. Phys. **A585** (1995) 450.

Figure Captions:

FIG. 1. Deep inelastic electron proton cross sections. The data points are from Whitlow, Ref. 18. The circle points are beyond our cuts and were not included in the χ^2 fit. (a) Scattering angle $\theta = 18^\circ$ with incident electron energy $\omega = 17.0$ GeV. (b) $\theta = 50^\circ$, $\omega = 19.5$ GeV.

FIG. 2. The structure function $F_2(x, Q^2)$. The data points are Whitlow's extraction of F_2 in Ref. 18.

FIG. 3. $R = \sigma_L / \sigma_T$. The data points are from Whitlow's extraction of R in Ref. 18. (a) $x=0.40$. (b) $x=0.55$. (c) $x=0.70$.

FIG. 4. The virtual photon asymmetry A_1 . The solid data points are from SMC, Ref. 11, and the open points are from E143, Ref. 9. The solid curve is the rest frame prediction for different u and d quark distributions, and the dashed curve is for equal u and d quark distributions.

FIG. 5. The spin dependent structure function g_{1p} . The experimental points in (a) are from SMC, Ref. 11, and in (b) from E143, Ref. 9. The dashed curve is for similar, and the solid curve for different u and d quark distributions.

FIG. 6. The rest frame prediction for the spin dependent structure function g_{2p} .

Fig. 1

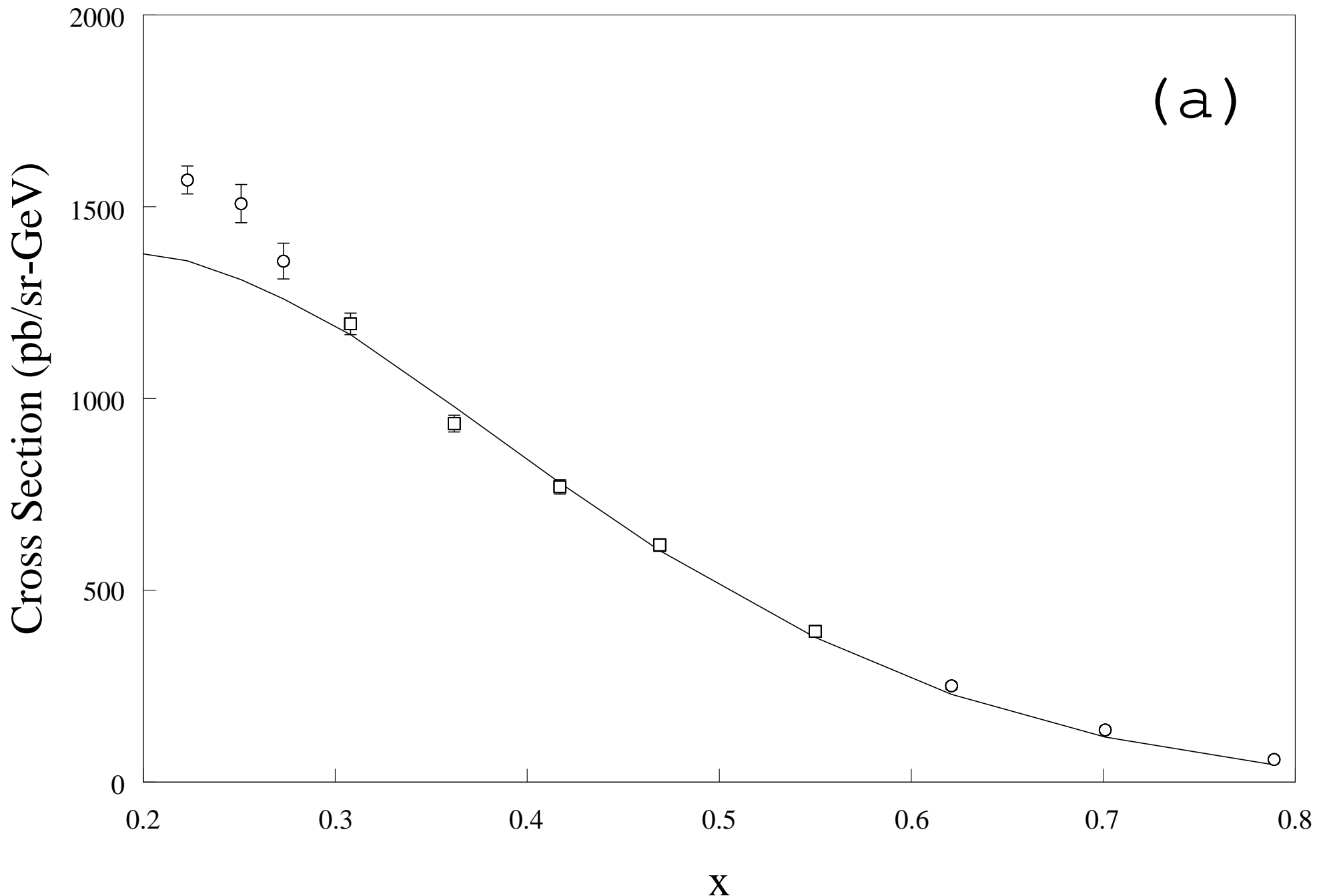


Fig. 1

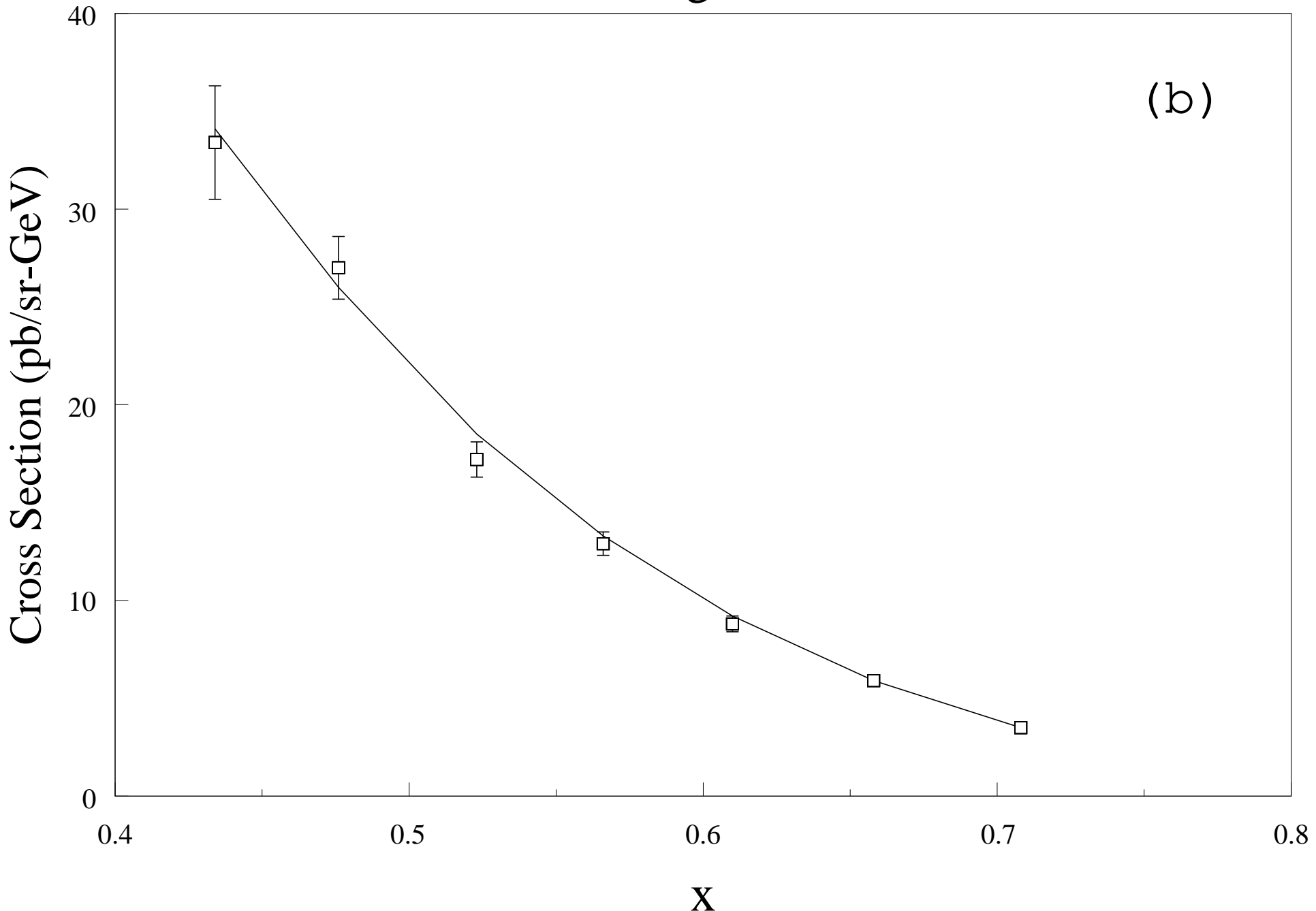


Fig. 2

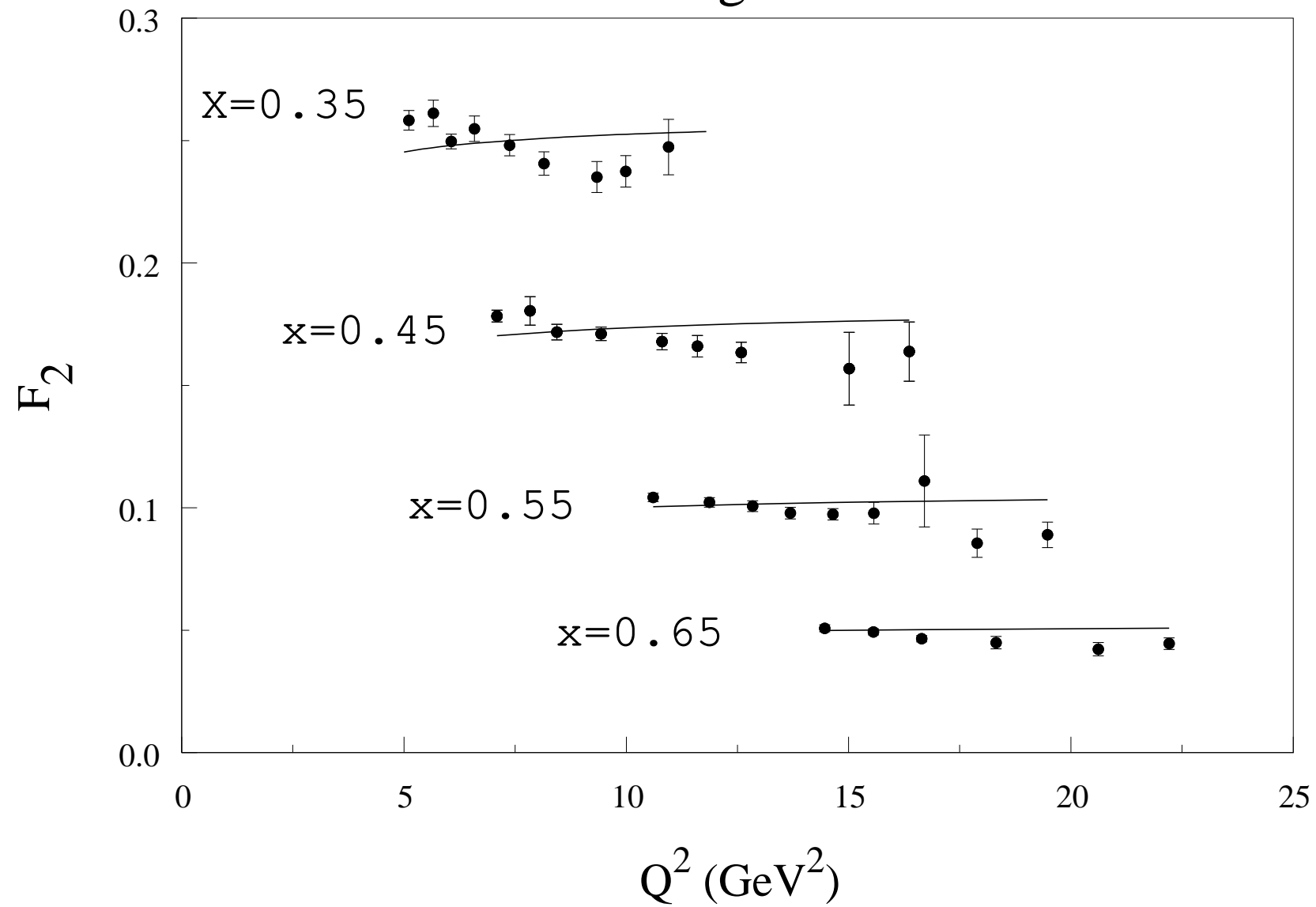


Fig. 3

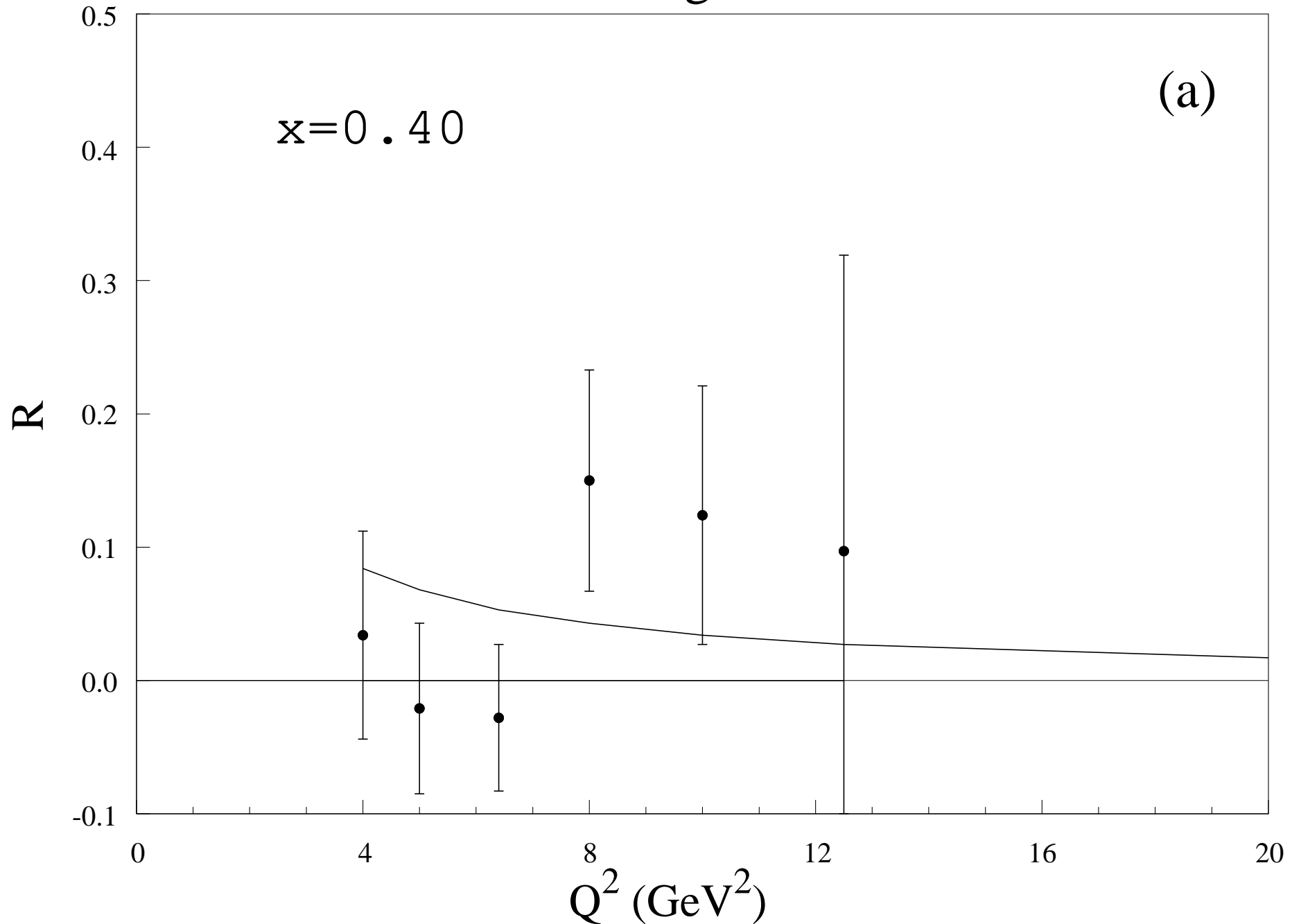


Fig. 3

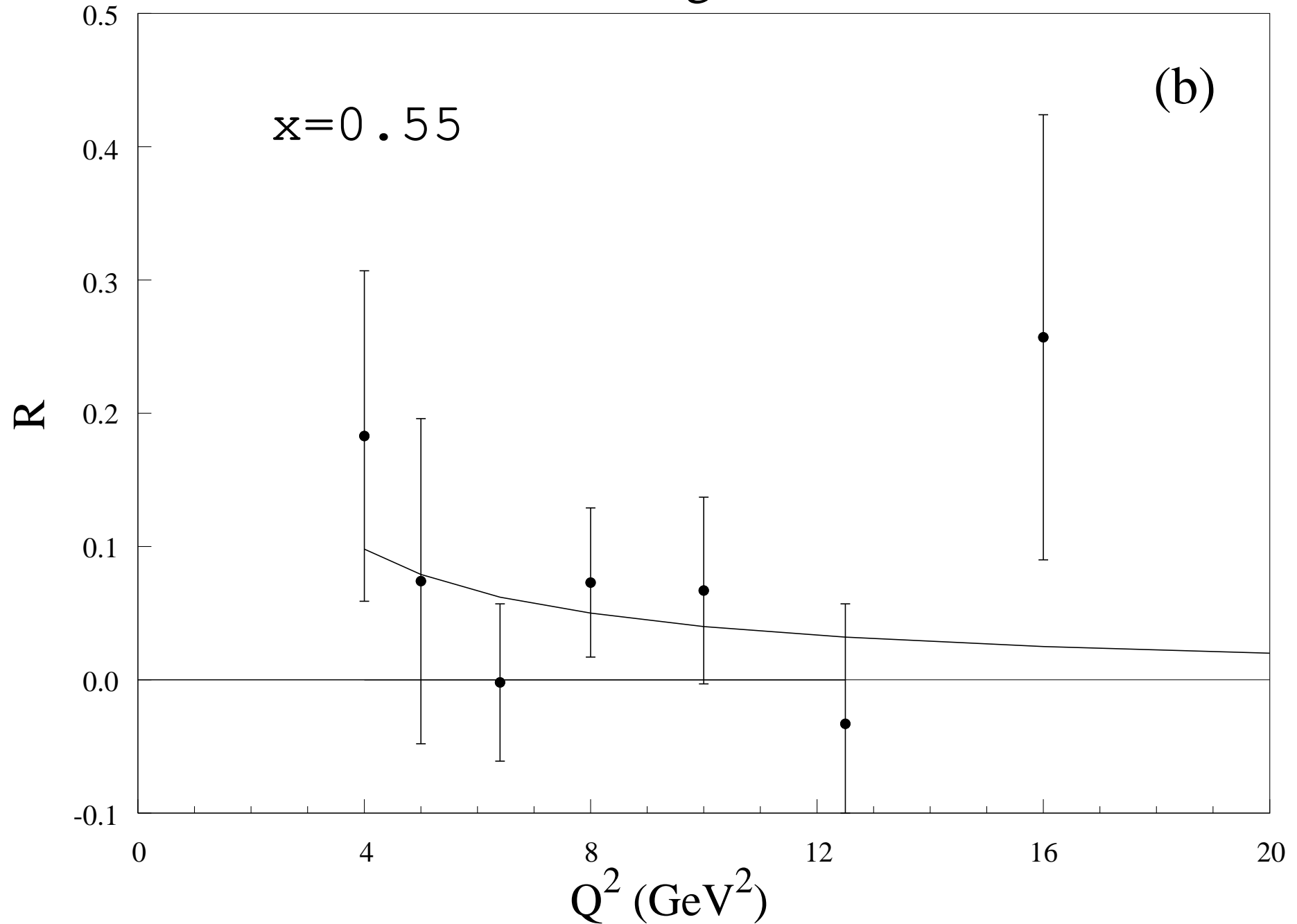


Fig. 3

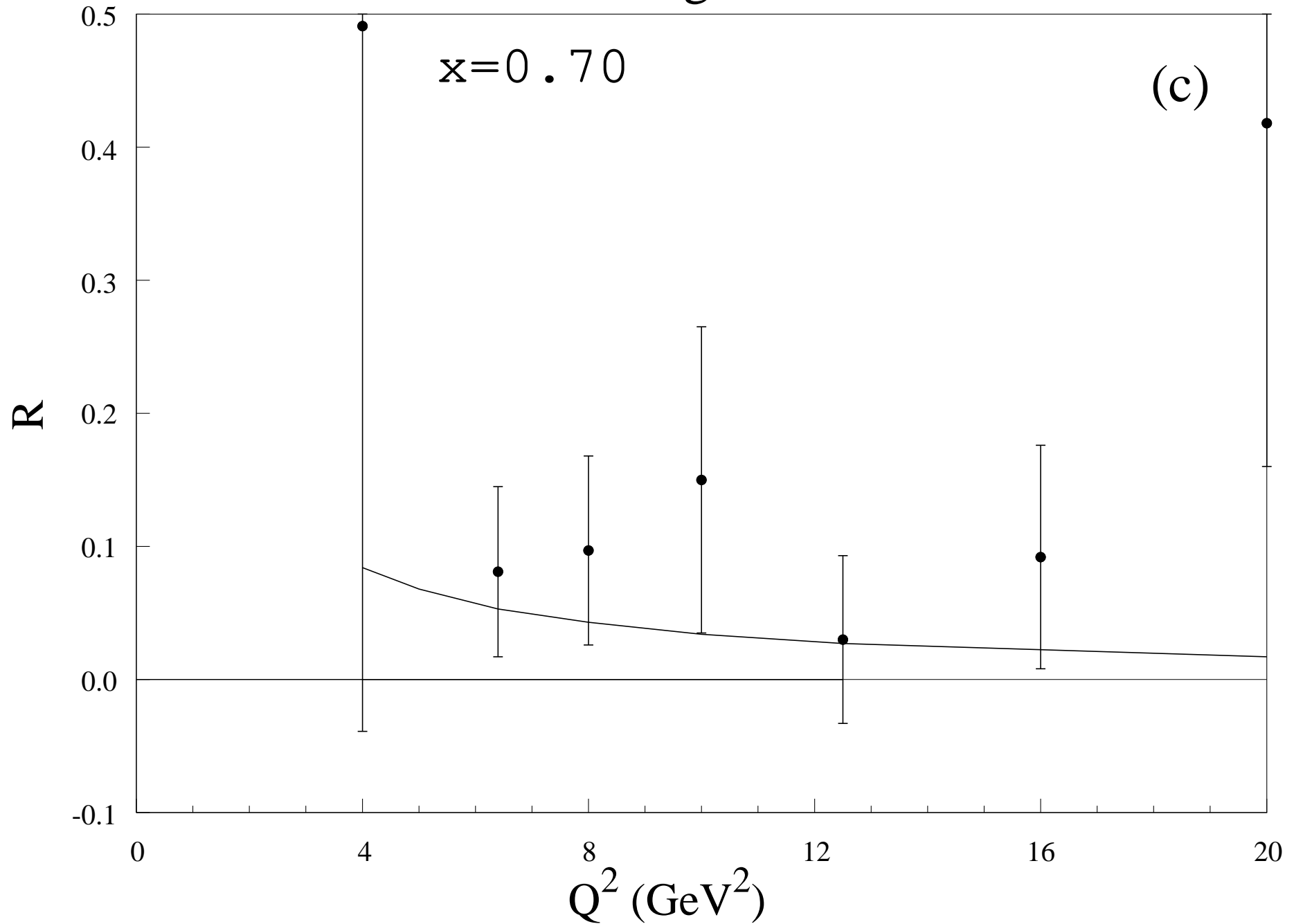


Fig. 4

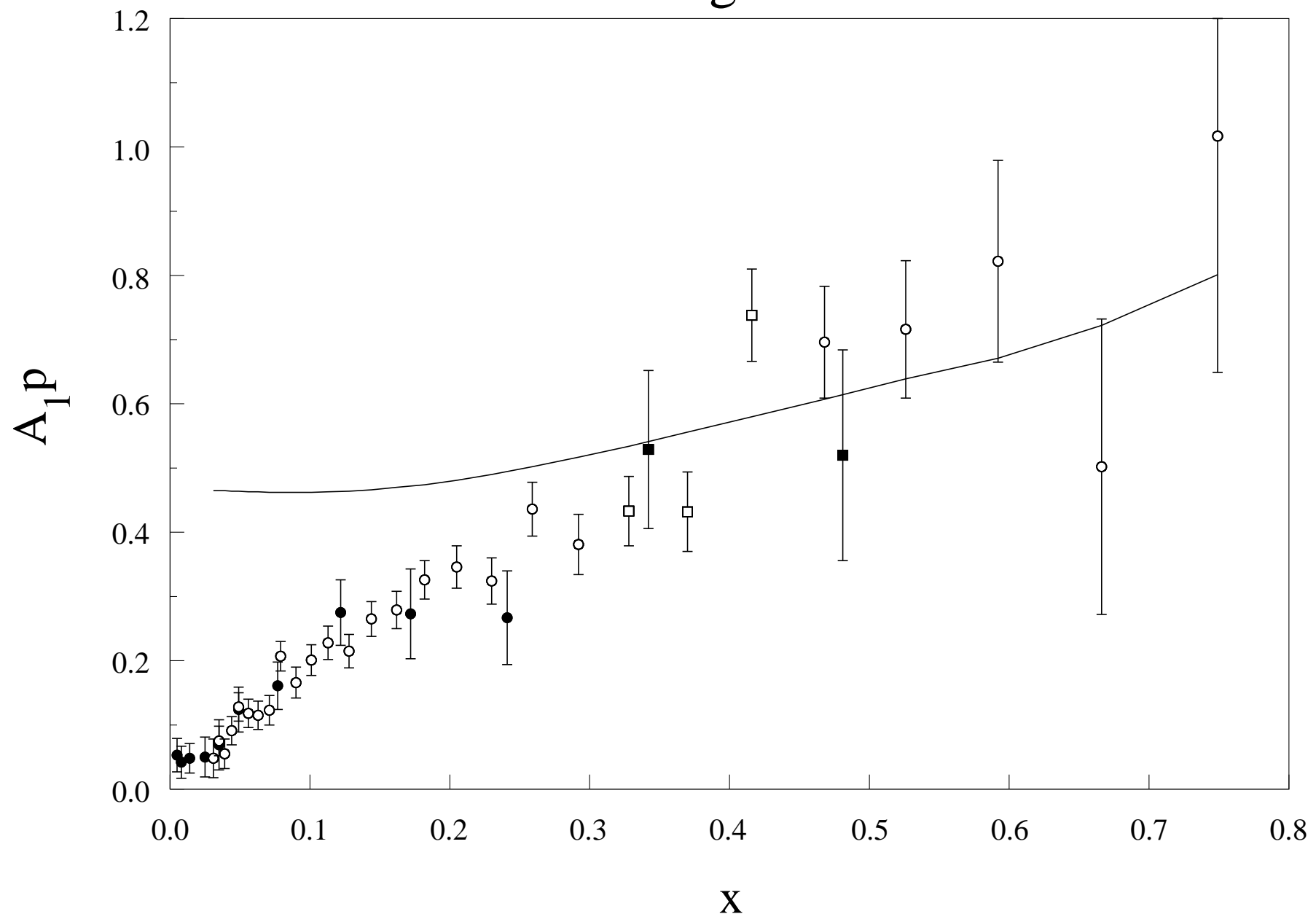


Fig. 5

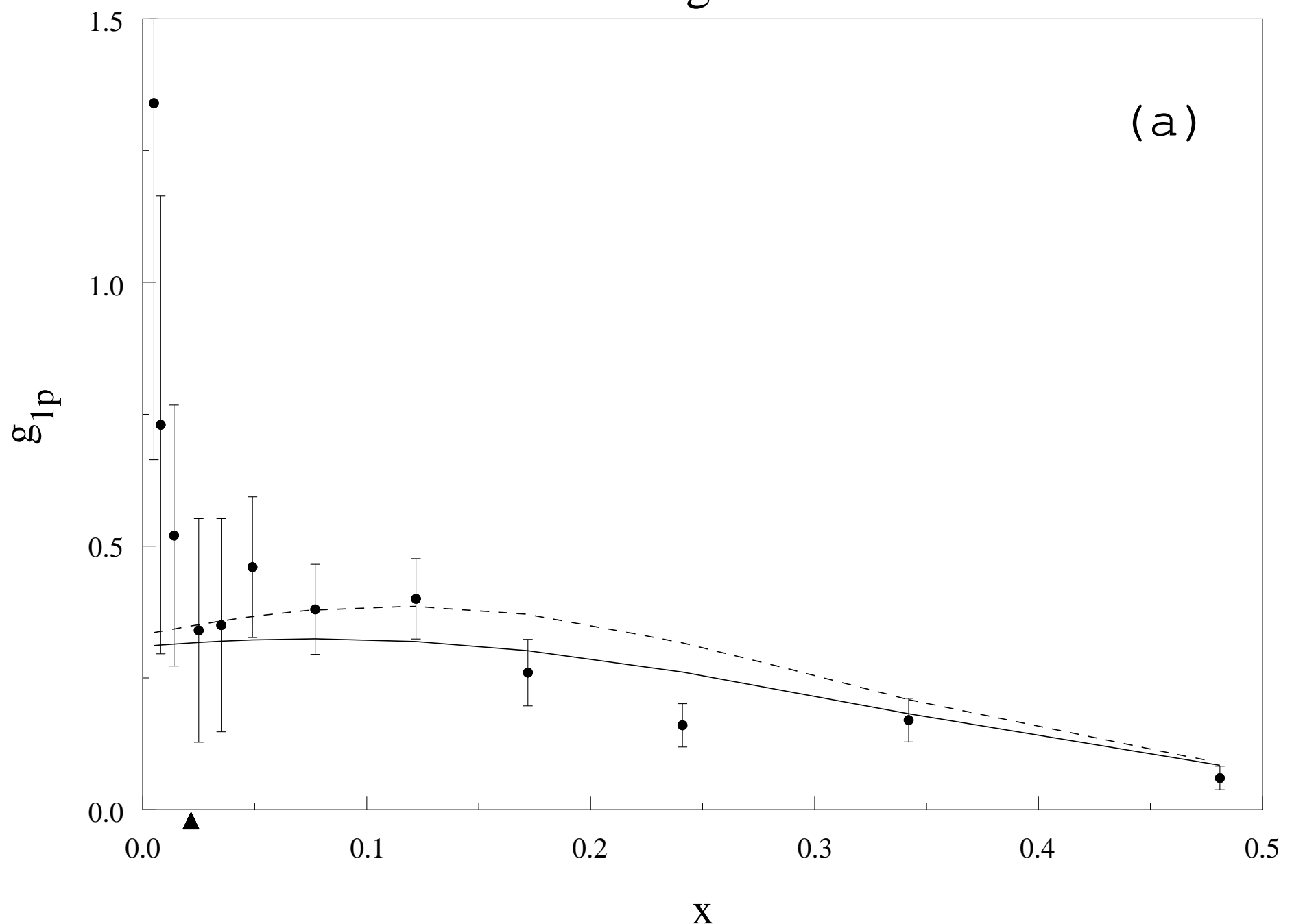


Fig. 5

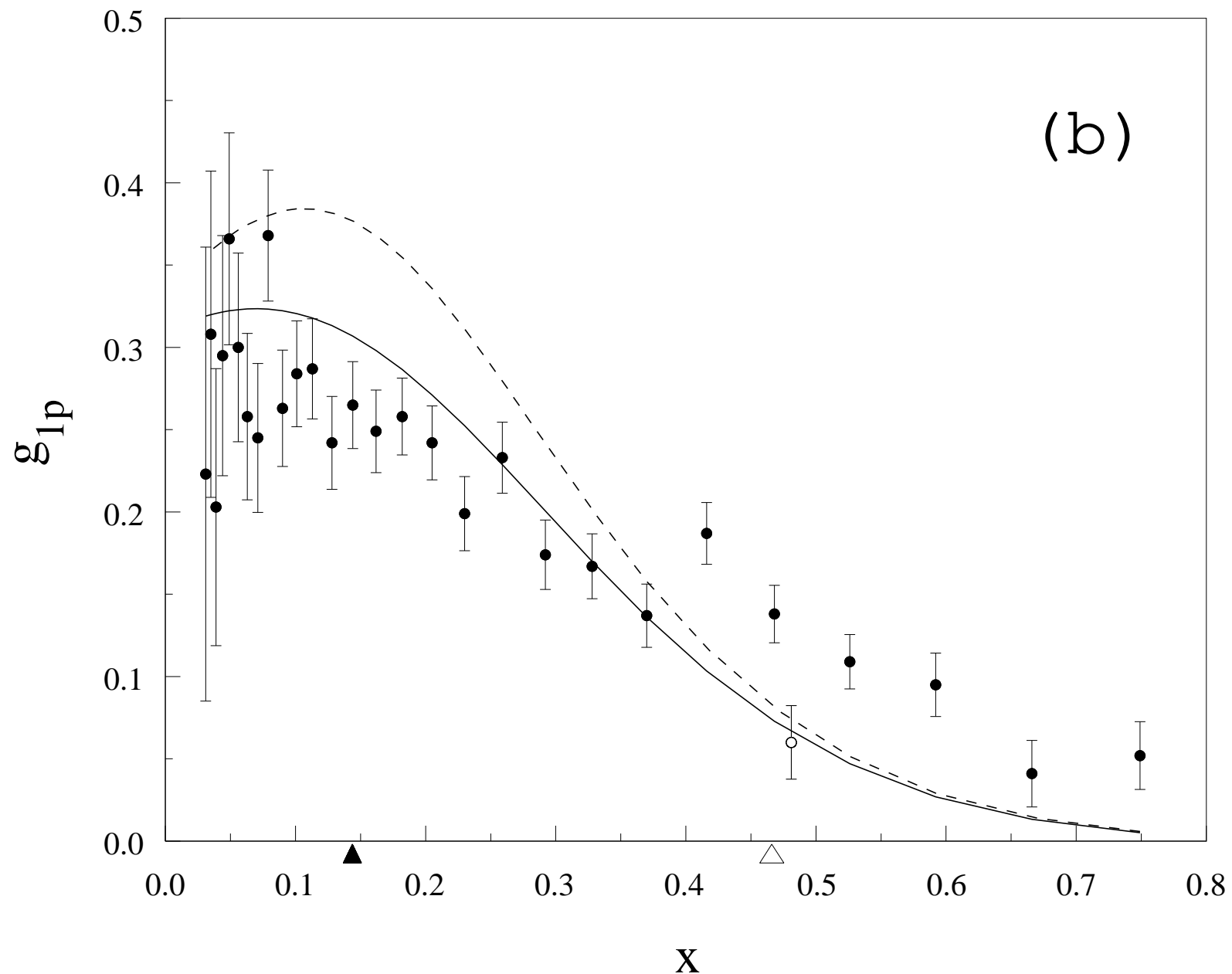


Fig. 6.

